Applied Surface Science 664 (2024) 160177

Contents lists available at ScienceDirect

Applied Surface Science

journal homepage: www.elsevier.com/locate/apsusc

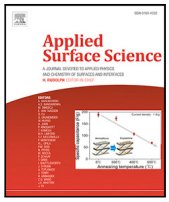

Full length article

Effects of surface chemical modifications on the adhesion of metallic interfaces. An high-throughput first-principle analysis

E. Poli *, M. Cutini, M.A. Nosir, O. Chehaimi, M.C. Righi *

Department of Physics and Astronomy, University of Bologna, 40127, Bologna, Italy

ARTICLE INFO

Keywords:
Adsorption
Adhesion
High-throughput
Density functional theory
Metal–metal heterogeneous interfaces

ABSTRACT

Chemical interactions between two surfaces in contact play a crucial role in determining the mechanical and tribological behavior of solid interfaces. These interactions can be quantified via the adhesion energy, a measure of the strength by which two surfaces bind together. A precise evaluation of how different species at solid contacts modulates their adhesion would be extremely beneficial for a range of different technological fields. In this work we have used and high-throughput approach to systematically explore the effects of the presence of non-metallic elements, at different concentrations, on the adsorption and adhesion energies of different metallic interfaces. Together with the databases for the adsorption and the adhesion energies, we calculated several other properties such as: charge transferred at the interface, d-band edge shift for the substrate, Bond order and the interfacial density redistribution for the hundreds of systems analyzed. These values were used to define different trends with respect to chemical and concentration parameters that could be useful for the development of engineered interfaces. We noticed how the adsorption of almost all non-metallic elements decreases the adhesion of solid interfaces, particularly Fluorine, Phosphorus and Sulfur. Interestingly, Carbon and Boron were the only two species that increased the adhesion instead.

1. Introduction

Solid–Solid interfaces are ubiquitous in natural and technological processes [1–3]. The mechanical behavior of such interfaces is dictated by an interplay between the macro [4] and microscopic properties [5] of the surfaces comprising the contact. In fact, while several physical processes govern friction and while their interplay is not fully understood [6] it is known that the chemical interactions of nano-asperities govern the friction coefficient [7,8]. In this context adhesive interactions are extremely relevant given the high surface to volume ratio at nano-asperity contacts. Adhesion is defined by the atomistic interactions of the mated surfaces. These interactions are modulated by several relevant factors such as chemical composition, crystal orientation and stacking, presence of adsorbates, impurities, defects and segregates [9–15]. In particular the presence of atomic adsorbates at metallic interfaces can modify the tribological and mechanical properties of interfaces with relevant implications in many technological fields such as metallurgy [16], nuclear fusion generator [17–19], automotive, catalysis [20], clean fuel deployment [21]. The phenomena influenced by the presence of adsorbates ranges from hydrogen embrittlement of steels [21,22] to superlubricity [23] to electrode adhesion [24] to different substrates and many more. A deeper knowledge of the effects of different adsorbates should allow the prediction and optimization of the mechanical and the tribological behavior of metallic interfaces, opening the possibility for applications where selected levels of adhesion and friction required are obtained through chemical engineering. The interplay between theoretical analysis and experimental evidence is pivotal in this direction. From a theoretical standpoint the advent of high-throughput software has dramatically enhanced the input that can be given to the experimental community to speed up/aide the discovery and testing of novel compounds with selected properties [25–29]. This approach hence has become a valuable tool for material advancements. In this paper we present an high-throughput study, based on an extension of the TribChem [30] program previously developed by our group, on how the absorption of non-metal atomic species at homogeneous metal–metal interfaces defines their adhesive and chemical properties. In particular we focus on how the presence of different adsorbates influences the Adsorption and Adhesion energies given their relevance in defining the tribological properties of an interface [31]. We also analyze how these central quantities are correlated to several other chemical descriptors/properties. The study of these systems gives us a perspective of the fundamental interactions at plays at the boundary between metallic interfaces and is a first step in order to move towards the comprehension of the physics of more heterogeneous interfaces.

* Corresponding authors.
E-mail addresses: emiliano.poli2@unibo.it (E. Poli), clelia.righi@unibo.it (M.C. Righi).

https://doi.org/10.1016/j.apsusc.2024.160177
Received 11 January 2024; Received in revised form 15 April 2024; Accepted 26 April 2024
Available online 30 April 2024
0169-4332/© 2024 The Authors. Published by Elsevier B.V. This is an open access article under the CC BY license (http://creativecommons.org/licenses/by/4.0/).

2. Computational methods

2.1. Tribchem

The high-throughput screening of the influence on adhesion of adatoms at homogeneous metal interfaces has been carried out using the TribChem software developed by our group. The technical details of the code are outlined in a separate paper [30]. TribChem role is to automate the creation of input files and geometries, submit and run the theoretical calculations, and finally collect and analyze the generated data in external databases. The code is mainly written in python and leverages Fireworks [32] and Atomate [33] as workflow managers. In addition TribChem is interfaced with Pymatgen [34] and MPInterfaces [35] that are used to create, manipulate and process the Input/Output operations. The DFT calculations are run by Tribchem using the Vienna Ab initio Simulation Package (VASP [36]). We used for all the simulations plane wave projector augmented wave (PAW [37]) basis and the Perdew–Burke–Ernzerhof [38] (PBE) -generalized gradient approximation of exchange correlation. Additional information regarding the energy cutoffs, number of k-points and the dimensions of the systems simulated can be found in Figure 1,2,3 and 4 of the Supporting Information.

2.2. Workflow outline

- Tribchem retrieves the structure for the material of interest from the Material Project database.
- The bulk structures are optimized converging their lattice parameters via a fit with the Birch-Murnaghan equation of state.
- The DFT energy convergence w.r.t the k-point mesh and the plane-wave cutoff is then evaluated via an automated set of calculations.
- The slabs of the materials selected are the obtained cutting the bulk along a input/user specified direction. In our specific case the slabs were cut along the most stable orientation of each crystalline structure: (111) for FCC crystal, (110) for BCC crystal and (0001) for HPC ones.
- The optimal slab thickness is selected via convergence of the surface energy.
- The adatom is added to the slab in the different high symmetry sites depending on the orientation of the surface (as an example: Long-bridge, short-bridge, or top for the (110) BCC crystals). The structures obtained are then relaxed until the convergence of the forces is minimized below 0.01 eV/Å.
- The lowest energy configuration is then selected and the adsorption energy with respect to the clean slab is calculated as :

$$E_{ADS} = \frac{(E_{SLAB+nAd} - nE_{Ad} - E_{SLAB})}{n} \tag{1}$$

where $E_{SLAB+nAd}$ is the total energy of the substrate covered by n adatoms, E_{Ad} is the energy of the isolated atom and E_{SLAB} is the energy of the clean substrate. E_{ADS} is then saved in the Adsorption Energies database.

- After, the full interface is built reflecting the slab (and not the adatom) through a mirror plane parallel to the slab surface. The mirrored slab is then placed at a distance along the z-axis equal to the interlayer spacing of the bulk. The total supercell is finally formed adding 15 Å of vacuum to decouple the Periodic Boundary Conditions (PBC) images along the z-direction. The structure is then relaxed along the z-axis until the convergence of the forces is minimized below 0.01 eV/Å.
- Subsequently, the mirrored slab is shifted laterally to match all the high symmetry positions of the lower slab and. Exploring the different shifts for which the high-symmetry points of the two surface match, and collecting the corresponding total energies, a 2-dimensional potential energy surface (PES) is built. The structure corresponding to the minima of the PES is then selected. Finally, this structure is fully relaxed until the convergence of the forces is minimized below 0.01 eV/Å.
- The adhesion energy is defined as the required energy (per unit area) to separate the slabs and create two free surfaces and is calculated as:

$$E_{ADH} = \frac{1}{A}(E_{12} - E_1^{Ad} - E_2) \tag{2}$$

where A is the in-plane supercell area, E_{12} si the total energy of the two slabs and the adatom in contact, E_1^{Ad} is the energy of the isolated lower slab with adsorbed the adatoms and E_2 is the energy of the isolated upper slab. E_{ADH} is then saved to the Adhesion Energy database.

- After, the charge density redistribution (ρ_{dist}) is calculated as:

$$\rho_{dist} = \frac{1}{2z_0}\int_{-z0}^{z0}\left|\frac{\rho_{12} - \rho_1^{Ad} - \rho_2}{A}\right| dz \tag{3}$$

where $2z_0$ is the interface distance, ρ_{12} is the planar average of the interface charge density ρ_1^{Ad} is the planar average of the charge density of the bottom slab with the adsorbed adatom and ρ_2 is the planar average of the charge density of the bottom slab for each specific system. ρ_{dist} is a metric to quantify the total amount of charge that is redistributed when an interface is formed bringing in to contacts the two surfaces comprising it [31]. ρ_{dist} is then saved to the charge density redistribution database.

- At the end, the post-processing analysis of the full systems calculations are run. In particular, the following properties are calculated for each system. The d-band edge :

$$\epsilon_d = \frac{\int_{-\infty}^{\infty} n_d(\epsilon)\epsilon d\epsilon}{\int_{-\infty}^{\infty} n_d(\epsilon) d\epsilon} \tag{4}$$

where ϵ_d is the center of d-projected DOS ϵ represents the Kohn–Sham eigenvalues and $n(\epsilon)$ is the calculated total d-PDOS. The work function :

$$WF = \phi - E_f \tag{5}$$

where WF is the work function of the total system (adsobate + metal surface) ϕ is the vacuum potential energy and E_f is the Fermi energy. We also calculate for each system the Density Derived Electrostatic Charges (DDEC) and the bond order that represents the number of chemical bonds between a pair of atoms. DDEC are evaluated with an atom in molecules charge partitioning scheme where the total electron density (n(r)) is partitioned into overlapping atomic densities (n_i(r)).

$$n_i(r) = \frac{w_i(r)}{\sum_k (w_k(r))} n(r) \tag{6}$$

The atomic partial charges are then computed by integrating the atomic electron densities over all space:

$$q_i = z_i - N_i = Z_i - \sum n_i(r) d^3 r \tag{7}$$

where N_i is the number of electrons assigned to atom i and z_i is its effective nuclear charge. Using the same approach, higher-order atomic multipoles may be computed as first-order, second-order, nth-order moments of the atomic electron densities. The weighting function in the DDEC method is described so that the atomic weights are simultaneously optimized to resemble the spherical average of n_i(r) and the density of a reference ion of the same element with the same atomic population N_i. In this way the DDEC charges are optimized to reproduce atomic chemical states and the electrostatic potential surrounding a material. Following this approach, the assigned atomic densities rapidly reach a converging multipole expansion of the QM electrostatic potential and the resulting atomic populations are chemically reasonable. Building on this charge partitioning the Bond Order of the different

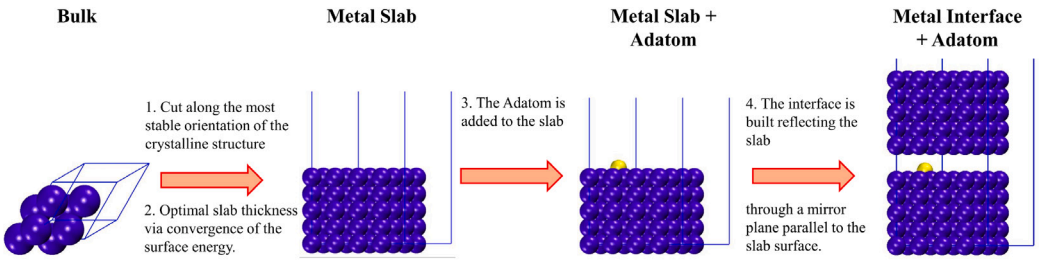

Fig. 1. Schematic of the process executed by Tribchem in order to build all the systems studied in this work.

atoms can be calculated. A more detailed explanation of these method is beyond the scope of this paper an the interested reader is remanded to Ref. [39,40]

In order to calculate the DDEC charges, Bond Order and d-band edges, we used the codes VASPKIT [41], and CHARGEMOL [39]. The capabilities of running post-processing analysis has not been fully implemented in the workflow yet and a more technical paper about these capabilities will follow. The full procedure outlined above is run for 1 × 1, 2 × 1, 2 × 2 cell dimensions (along the a and b cell axis respectively) considering in each case only one adatom per system and simulating in this way three different coverages, $\theta = 1.0$ monolayer (ML), $\theta = 0.5$ and $\theta = 0.25$, respectively. A schematic of the system building process is shown in Fig. 1

2.3. Substrates and adatoms choices

The substrates choice was driven by our previous work (and hence the availability of the E_{adh} and ρ_{dist} data) on the clean homogeneous interfaces of these metals. The series of substrates analyzed comprises of: Ag, Al, Au, Cr, Cu, Fe, Ir, Mg, Mo, Ni, Pt, Ti, W, and Zn. These metals were chosen given their technological relevance both in pure [42] form and as alloys components, and the fact that they constitute a representative set of transition metals with different d-orbital occupations. In fact, in real world application metals are separated from the atmosphere by oxidized surfaces which are largely chemically inert. However, the tribological process usually wears away these exterior layers exposing the fresh material underneath resulting in accelerated tribochemical reactions [43]. Recent examples in literature have confirmed these observations such as how freshly scratched gold surfaces resulted in enhanced chemisorption [44] or how nascent steel surfaces can induce the formation of iron phosphide tribofilms [45–47]. In addition Mg and Al were also considered as limit cases of metal which reactivity is dictated by s and p-orbitals. The adatom selection comprises of all reactive non-metals from the first second and third period (Cl excluded). Boron was also included given its relevance in previous tribological studies.

3. Results and discussion

The database of the adsorption energies for the different substrates with the different adatoms adsorbed on top and the one of the adhesion energies of the interfaces with the adatoms intercalated are shown in Fig. 2 top and bottom panel respectively. The data are reported for all the three different coverages considered.

3.1. Adsorption energy analysis

Several general trends are observable regarding the adsorption energies:

(i) The substrates with low filling of d-band are the most prone to adsorb adatoms (see Fig. 2, top panel). This trend is consistent with d-band center theory [48] for adsorption on metals for which the higher the d states are in energy relative to the Fermi level, the higher in energy the antibonding states are hence the stronger is the bond. This explain the lower propensity of noble metal and Zinc to adsorb different species [49,50] with energies in the order of 4 - 2 eV/atom for the 25% coverage, 3 - 2 eV for 50% coverage and 2 - 1 eV for 100% coverage. Conversely, the adsorption energies for the adatoms on the other substrates increase with the decrement of the d electrons. These trends were all confirmed by the d-band edge values calculated for all system (Table 5 Supporting information). Aluminum (that has only one p electron) shows adsorption energies that are comparable in magnitude with the ones of low filled d-bands substrates. It also shows (and Magnesium too) similar energetic trends to the low filled d-bands substrates with a high propensity to adsorb C, O and N. The case of Magnesium is difficult to evaluate since for several systems the adsorbed species percolates into the surface structure, in particular C, N and O. This is probably due to the high reactivity of the alkaline-earth metals and the large lattice parameter along z of Mg that allows for easier percolation.

(ii) The most favorable adatom to adsorb depends both by the substrate and the coverage of the system (see Fig. 3a). As an example for Tungsten the most favorable species to adsorb at low coverage is Carbon but as soon as we consider $\theta = 0.5$ and $\theta = 1.0$ Oxygen becomes the more stable adatom on the substrate. In only four systems the coverage does not influence the most favorable species adsorbed. These are: Pt/C, Ag/F, Cr/C and Al/O. In general the species with highest Adsorption Energy are the ones with smaller atomic radii exception made for hydrogen (i.e. C,N,O and F). It is notable how at higher coverages the adsorption of Fluorine becomes more advantageous with respect the other adatoms.

(iii) H is the least energetically favorite species to adsorb on the different substrates except for high concentrations cases where S and P are instead the least favorite (especially on coinage metals). Fig. 3b in fact highlights how at $\Theta = 0.5$ and 0.25 H is generally the least favored adatom on the different surfaces.

(iv) Fig. 3c show the average change in Adsorption energy passing from $\Theta = 1.0$ to 0.5, $\Theta = 1.0$ to 0.25 and $\Theta = 0.5$ to 0.25. It can be seen that for atoms with smaller atomic radii the changes in E_{ads} are smaller (i.e. the gain in energy due to adsorption is less coverage dependent). In particular for Hydrogen the adsorption energies remain on average the same, in the concentration range analyzed. B, C, S and P E_{ads} show instead a marked dependence by the coverage. Decreasing the coverage in these cases in fact leads to a drastic increase of the adsorption energies that seems to be correlated to a shortening of the distance between the ad-atoms from the surface (see Fig. 2, central panel). Fig. 3d shows in particular how the B, C, P and S are on average 0.3-0.2 Å further away from the substrate at $\Theta = 1.0$ with respect to $\Theta = 0.25$. For the other species the distance from the substrate remains almost the same exception made for F. These trends can in part be explained calculating the Bond Order between the adatoms and the different species present in the system. (see Fig. 3e,f) For B, P, S (and in a more limited way C) the increment in coverage leads to an increment in the Bond Order of the adatoms with their periodic images (Fig. 3e) and a decrement of the total Bond Order with the atoms comprising the substrate (Fig. 3f). This implies that when the concentration of the adatom adsorbed at the surface is increased the species with larger atomic radii tend to form stabilizing bonds among

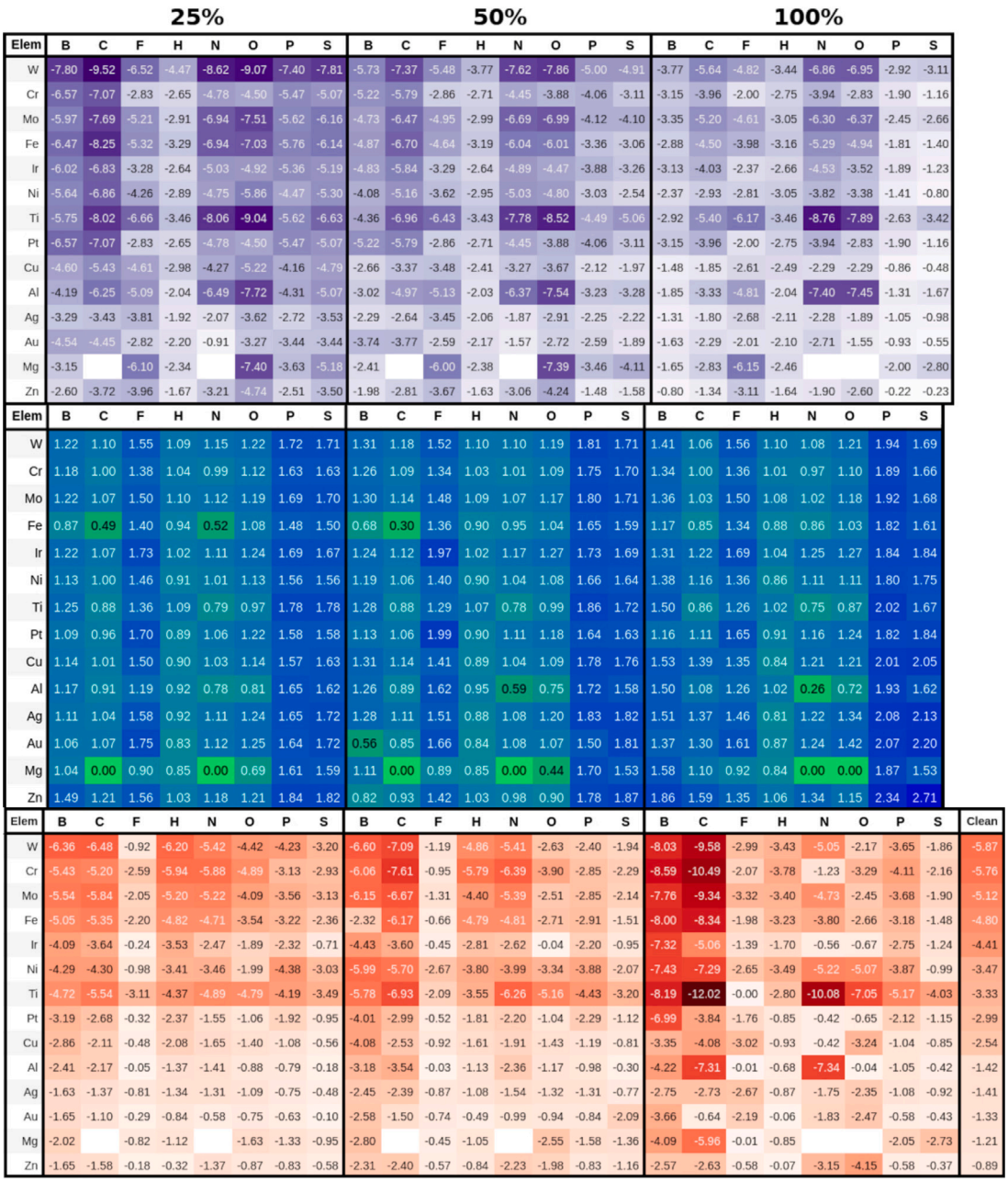

Fig. 2. Adsorption energy in eV (top panel), vertical distance along z between the adatom and the xy-plane of the substrate slab in Å (middle Panel) and adhesion energy in (J/m^2) (bottom Panel) for 25%, 50% and 100% coverages. Empty squares (or with 0 value) indicates when the atomic adsorption is not stable. In this cases, the adsorbate percolates into the surface structure. For the adhesion energies the clean interfaces values calculated in Ref. [51] are reported in the Column "Clean". In all cases darker shades are related to higher adsorption and adhesion energies.

themselves and decrease the interaction (i.e. form less bonds) with the substrate.

(v) Regarding the DDEC charge analysis we evaluated the net charge transferred to the adatom from the surfaces comprising our systems. In this analysis a net negative charge indicates a transfer of electronic density to the adatom and a net positive charge is index of a depletion of electronic charge on the species adsorbed(see Figure 6 in the Supporting Information for the full database). It can be observed that systems presenting higher adsorption energies also present the bigger net negative charges on the substrates adatoms and the adatoms. This shows that in systems where there is a relevant charge (electronic density) transfer from the surface to the adatom tend to adsorb in a more stable configuration. The magnitude of the charge transfers seems to be especially significant in the two non-transition metal case and Titanium. It can be also observed that for Phosporus in some limited cases the electronic density is transferred from the adatom to the metal surface (Boron also has net charges near 0 in some cases). This behavior possibly reflect the fact that these two species are the ones with the lowest electronegativity of the set we considered for the adatoms.

3.2. Adhesion energy analysis

Regarding the adhesion energy database (bottom panel Fig. 2) we notice that:

(i) The presence of adatoms leads in almost all cases to a reduction of the adhesion energy. The important exceptions to this trend are Boron and Carbon (and hydrogen for 110 surfaces) that at low Θ slightly increase the adhesion energy and at higher coverage highly

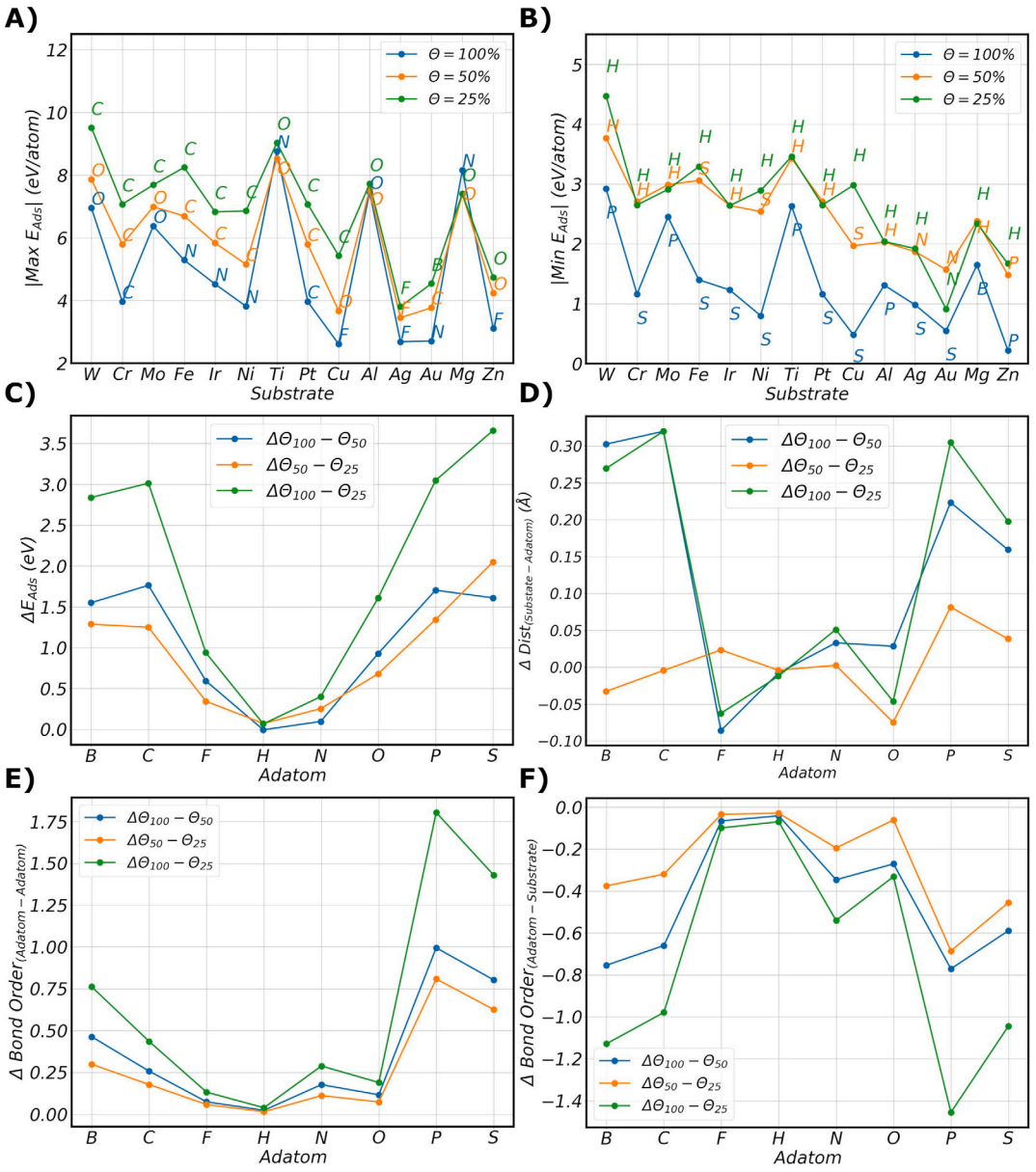

Fig. 3. Panel A: Maximum absolute value of the Adsorption Energy (E_{Abs}) for each substrate considered with respect to the coverage. The adatom for which the Maximum Adsorption Energy is obtained is specified in the label above the data-point. Panel B: Minimum absolute value of the Adsorption Energy (E_{Abs}) for each substrate considered with respect to the coverage. The adatom for which the Minimum Adsorption Energy is obtained is specified in the label above the data-point. Panel C: Average difference in Adsorption Energy between different coverage for all the adatoms considered. Panel D: Average change in distance from the substrate between different coverage for all the adatoms considered. Panel E: Average change in Bond Order between adatoms considering different coverage. Panel F: Average change in Bond Order between adatoms and the substrate considering different coverage.

increase it (Hydrogen does not follow this trend for higher concentrations). From Fig. 4a it can be seen that for almost all cases (Mg, Zn and Al excluded) at high concentrations Boron and Carbon are in fact the adatoms that produce the highest adhesion between surfaces(i.e. lowest adhesion energy). Both these species are known for their flexibility in forming bonds [52–55], hence we can hypothesize that at a certain concentrations such behavior could lead to the formation of stronger interactions at the interface w.r.t the other adatoms. However, given the recent literature highlighting the lubricant properties of graphene [56,57] it is important to specify how the systems described in our simulations present a very different chemistry from the graphene case. In fact in our system the carbon atoms are adsorbed at distances where they cannot form stable bonds hence they are more prone to interact with the substrate and transfer charge/electronic density. Our systems geometries (at least using the current workflow setup) are more suited to be compared to the addition of additive in alloys and metalworking. Several studies can be found where the addition of Boron and Carbon lead to an increment of the material strength, toughness, and high wear resistance [58–63]. Many of these works focused on Iron based systems [58,59] but even the other examples show that as long as the presence of these elements is interstitial all the previously listed properties are enhanced. In particular, boron is nowadays commonly added to many structural alloys primarily as a grain-boundary strengthener [60,61].

(ii) Fig. 4b shows instead that the lowest adhesion between surfaces (i.e. highest adhesion energies) are obtained for systems with Fluorine or Sulphur adsorbed at the interface. This is consistent with the fact that sulfur [64,65] and fluorine compounds are at the basis of several industrial lubricant additives. Several reports in literature also suggest F as promising adhesion-reducing element at interfaces [66–68] and

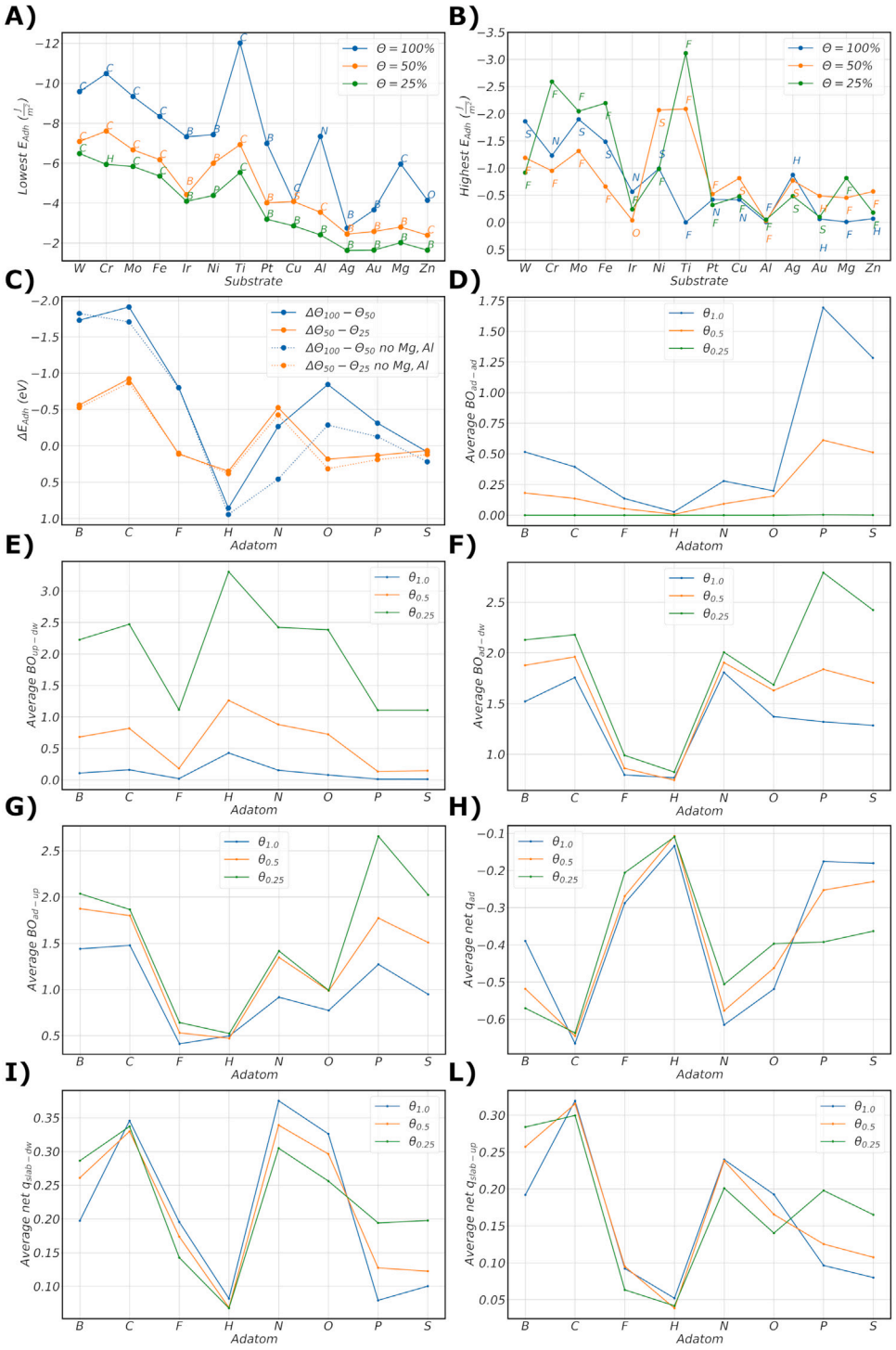

Fig. 4. A: Maximum absolute value of the Adhesion Energy (E_{Adh}) for each substrate considered with respect to the coverage (Θ). The adatom for which the Maximum E_{Adh} is obtained is specified in the label above the data-point. B: Minimum absolute value of E_{Adh} for each substrate considered with respect to the Θ. C: Average difference in E_{Adh} between different Θ for all the adatoms considered. The dotted line represent the same analysis executed without considering Mg and Al. D: Average Bond Order (BO) between adatoms w.r.t different Θ. E: Average BO between upper and lower slab of the interface for each adatom considered w.r.t different Θ. F: Average BO between adatom and the lower slab of the interface for each adatom considered w.r.t different Θ. G: Average BO between adatom and the upper slab of the interface for each adatom considered w.r.t different Θ. H: Average net charge for each adatom at the interface. I: Average net charge of the lower slab for each adatom case w.r.t different Θ. L: Average net charge of the upper slab for each adatom case w.r.t different Θ.

could be also connected to the hydrophobicity of fluorinated interfaces (such as Teflon). Our findings also confirm previous results for S that is know for its lubricating properties, especially at Fe interfaces [69].

(iii) It is interesting to observe how the difference in coverage plays a less clear role for adhesion interactions w.r.t. the adsorption energies case (see Fig. 4c). In fact for F, N, O and P there is on average a decrement in adhesion energy (i.e. increment in adhesion strength) going from $\Theta = 0.5$ to $\Theta = 1.0$ even if the overall E_{Adh} value remains higher than in the clean interface case (i.e. less adhesive interface). On the contrary, the adhesion energy is increased (i.e. decrement in

adhesion strength) if we increase the coverage passing from $\Theta = 0.25$ to $\Theta = 0.5$ (exception made for B, C and N). The only two adatom species for which the Adhesion decrease constantly (i.e.constant increase of E_{Adh}) with and increment of the coverage are Sulfur and Hydrogen. Such trend has also relevant technological implications since hydrogen embitterment is an important challenge to resolve in order to enable hydrogen to become a wide-spread fuel option [70].

(iv) To further explore the reasons behind these non-linear trends of the Adhesion energies w.r.t. the atom coverage we analyzed the Bond Order (BO) data for all the different species comprising the interfacial systems. Fig. 4d shows the average BO between the adatoms adsorbed at the interface. It can be seen that the trend are similar to the adsorption cases where an increment in the adatom concentration leads to rise in the number of bonds formed between the adatoms. This trend is shared by all the adatoms species other than H, that given its lone valence electron tends to remain in the same state for all the Θ considered. A similar behavior is noticed for Flurione although its disposition to scarcely interact with the other adatoms could be ascribed to the strong electrostatic interaction between them. As in the adsorption cases Phosphorus, Sulfur, and in a more limited way Boron and Carbon, are the species that form the stronger bonding between their adatoms. Panel E in Fig. 4 displays the average BO between the upper and lower slabs comprising the interfaces w.r.t. to the species adsorbed. It can be seen that for really high concentrations of the adatoms (i.e. $\Theta = 1.0$) the slabs do not form any bonding between them exception made for the hydrogen and nitrogen cases. The decrease in adatom coverage leads to a marked increment of the BO between slabs excluded the F,S,P cases. It follows that the intercalated species that promote a decrease in adhesion (i.e. increase in adhesion energy) are the ones that better prevent the formation of bonding interactions between the interface slabs. This data is supported by the distance analysis between the different slabs forming the interfaces (see Supporting info Figure 12, 13 and 14). In fact the trends observed for the BO between slabs are the same as the ones found for the distance calculated between them. The opposed surfaces are at larger distances for cases where the BO between them is lower (F,P,S) and at closer contact for systems where the BO is bigger (B,C,O). These finding allow us define a clearer picture of the interactions/processes determining the adhesion at the different interfaces. To further confirm these observations we calculated the Pearson correlation coefficients for the Bond Order between slabs and the adhesion energy and for the distance between slabs and the adhesion energy (see Supporting Information Figure 15). Both the quantities considered strongly correlate (negatively and positively respectively) with E_{adh} highlighting their importance in interpreting the physics happening the interface. In addition to these observations, Fig. 4f and g show us the average BO between the adatoms and the upper an lower slab. B,C, P and S tend on average to form a bigger number of bonds with the metal surfaces, while F and H are almost non bonded especially in the $\Theta = 1.0$ case. From the same data, we can also see that the number of bonds formed with the lower slab (on which the adatom is absorbed) is slightly bigger than the BO number for the upper slab for all the adatoms species. This asymmetry is interestingly much less marked in the B and C cases where the adhesion is of the interface is increased. The sum of these results/analysis shows us that while the bonding interactions play a crucial role in determining the behavior of our interfaces they are not sufficient to derive a full picture of the physics defining their properties.

(v) Additional information about the reasons behind these multivariate trends of the E_{Adh} with respect to the coverage can be deduced by the charge analysis of the different components of the systems simulated. Fig. 4h,i,l show the average net DDEC charge of the adatom (Panel h), down slab (Panel i) and up slab (Panel l) w.r.t to the different adatom coverage and adatoms species considered. The adatoms electronic (negative) net charge increases, for C, H, F, N and O at higher coverage while the opposite change is observed for B, P and S. In all the systems the accumulation (loss) of electronic density on the adatoms generate a loss (increment) in negative charge on the up and down (i.e. the surfaces on which the adatoms are adsorbed) slabs. In similar fashion to the BO analysis, the redistribution of the charge between the two slab is not symmetrical and leads to non trivial electrostatic pattern at the interface. The electronic density redistribution also seems to play a role in defining the adhesion between the metal surfaces. In fact the graphs show that for B, C, N and O the net charges localized on the different components of the system are bigger in magnitude leading to stronger electrostatic interactions between them and in general (although some deviations from this trend especially for O and N can be observed) to bigger adhesion interactions (i.e. lower adhesion energies). On the contrary for F, P and S present a smaller net e^- charge on the adatoms (and a smaller positive charge on the slabs) resulting in a diminished repulsive electrostatic interaction between the components of our interfaces. This diminished interaction probably contributes to higher E_{Adh} (i.e. lower adhesion). The H case is different from all the others since the change in surface coverage does not lead to big changes in the charge transferred between the slab and the adatom, hence the electrostatic interactions remain almost the same and the adhesion behavior is mainly dictated by the bonding between the up and down slabs. These observations about the charge redistribution further highlight how the adhesion energy is defined case by case by the interplay between bonding and electrostatic interactions, that is determined itself by the microscopic environment/morphology at the interface. Such variety further underlines the necessity for careful atomistic simulations of the interface environment/morphology when study these systems.

3.3. Interfacial density redistribution analysis

The interfacial density redistribution data should aid us in further understanding the phenomena underpinning the adhesion behavior at the interface. Previous studies [31,51] have shown the linear relationship between ρ_{redist} and E_{adh} for clean interfaces. Should this relationship hold(or another clear trend be found) for our interfaces with adatoms it will help us understanding how the different adatom atomic species modulate the density at the interface and in turn determine their effect on the adhesion energy. ρ_{redist} shows similar trends (see Image 5) to the adhesion energy w.r.t to the Adatom species in fact, for all the adatoms where the adhesion was drastically reduced (P,S and F) we can observe how the ρ_{redist} values are smaller. This indicates a smaller redistribution of the charge density at boundary that in previous work has been correlated to lower adhesion and hence friction [31]. ρ_{redist} values generally remain similar at lower concentrations ($\Theta = 0.25$ and 0.5) and than increase at full coverage. This behavior could be dictated by the fact that the higher the concentration of the adatoms the bigger (on average) is the charge transferred with the two slabs (see Fig. 4). The only two species that do not follow this trend are H, N and to a lesser extent O. In particular the presence of hydrogen results in high values of ρ_{redist} at low concentration but the electronic redistribution between metallic slabs progressively decreases at higher coverage. Almost all the values of ρ_{redist} calculated for the 25%–50% concentrations are lower with respect to their clean reference. This in principle respect the linear correlation observed between E_{Adh} and ρ_{redist} in previous work [31,51]. In fact the lower the adhesion the lower the charge density redistribution. However for B and C at $\Theta = 0.5$ decoration the ρ_{redist} value is smaller that the clean interface one but E_{adh} is bigger. This deviation from the trend is even more evident at full concentration where especially for d-metal with low filled orbitals. These deviations support our previous observations for the Adhesion Energies and further highlights how the presence, concentration and geometry of the adatoms has to be factored in the analysis of interfacial charge density redistribution. In fact it seems that the concentration of the adatoms together with the charge transfer they induce and the consequent electrostatic interactions at the nanoscale result in a non-trivial energetic picture with respect to the Adhesion interaction.

	25%								50%								100%								
Elem	B	C	F	H	N	O	P	S	B	C	F	H	N	O	P	S	B	C	F	H	N	O	P	S	Clean
W	0.0182	0.0188	0.0045	0.0211	0.0213	0.0182	0.0046	0.0083	0.0135	0.0149	0.0050	0.0187	0.0147	0.0123	0.0066	0.0070	0.0139	0.0162	0.0122	0.0130	0.0141	0.0084	0.0102	0.0083	0.0200
Cr	0.0187	0.0216	0.0115	0.0225	0.0166	0.0088	0.0071	0.0096	0.0128	0.0140	0.0065	0.0171	0.0134	0.0138	0.0077	0.0076	0.0217	0.0161	0.0109	0.0135	0.0063	0.0125	0.0100	0.0095	0.0270
Mo	0.0167	0.0176	0.0080	0.0225	0.0182	0.0151	0.0112	0.0102	0.0132	0.0147	0.0053	0.0163	0.0145	0.0121	0.0064	0.0069	0.0140	0.0155	0.0126	0.0121	0.0147	0.0088	0.0101	0.0083	0.0210
Fe	0.0136	0.0152	0.0116	0.0176	0.0156	0.0108	0.0076	0.0062	0.0121	0.0114	0.0046	0.0126	0.0119	0.0093	0.0058	0.0052	0.0156	0.0136	0.0111	0.0098	0.0133	0.0114	0.0092	0.0076	0.0220
Ir	0.0068	0.0085	0.0026	0.0103	0.0094	0.0068	0.0063	0.0035	0.0083	0.0065	0.0047	0.0075	0.0057	0.0018	0.0067	0.0045	0.0116	0.0098	0.0095	0.0068	0.0067	0.0065	0.0078	0.0061	0.0120
Ni	0.0092	0.0114	0.0074	0.0128	0.0120	0.0111	0.0050	0.0040	0.0089	0.0073	0.0086	0.0096	0.0109	0.0097	0.0072	0.0055	0.0169	0.0144	0.0135	0.0100	0.0173	0.0177	0.0101	0.0087	0.0160
Ti	0.0153	0.0118	0.0149	0.0169	0.0176	0.0169	0.0116	0.0120	0.0137	0.0165	0.0087	0.0154	0.0149	0.0137	0.0072	0.0070	0.0160	0.0182	0.0019	0.0104	0.0149	0.0102	0.0100	0.0126	0.0170
Pt	0.0059	0.0073	0.0031	0.0088	0.0077	0.0057	0.0049	0.0039	0.0062	0.0048	0.0045	0.0073	0.0075	0.0049	0.0045	0.0033	0.0100	0.0100	0.0098	0.0063	0.0046	0.0055	0.0074	0.0062	0.0090
Cu	0.0035	0.0041	0.0028	0.0098	0.0068	0.0065	0.0019	0.0017	0.0063	0.0049	0.0047	0.0087	0.0045	0.0046	0.0039	0.0031	0.0121	0.0108	0.0111	0.0075	0.0107	0.0127	0.0062	0.0062	0.0100
Al	0.0057	0.0083	0.0006	0.0085	0.0095	0.0058	0.0031	0.0024	0.0051	0.0101	0.0008	0.0063	0.0079	0.0045	0.0036	0.0030	0.0107	0.0210	0.0004	0.0041	0.0168	0.0015	0.0055	0.0070	0.0090
Ag	0.0024	0.0034	0.0047	0.0059	0.0040	0.0056	0.0012	0.0017	0.0036	0.0044	0.0045	0.0055	0.0044	0.0059	0.0023	0.0025	0.0091	0.0082	0.0088	0.0055	0.0048	0.0099	0.0058	0.0055	0.0050
Au	0.0020	0.0031	0.0035	0.0044	0.0040	0.0039	0.0018	0.0007	0.0008	0.0070	0.0050	0.0034	0.0065	0.0034	0.0023	0.0025	0.0064	0.0044	0.0092	0.0028	0.0079	0.0103	0.0048	0.0053	0.0050
Mg	0.0058		0.0053	0.0064		0.0064	0.0047	0.0042	0.0047		0.0036	0.0050		0.0054	0.0043	0.0040	0.0074	0.0120	0.0003	0.0046			0.0086	0.0122	0.0080
Zn	0.0039	0.0042	0.0029	0.0036	0.0040	0.0042	0.0035	0.0029	0.0040	0.0055	0.0046	0.0049	0.0075	0.0067	0.0038	0.0047	0.0078	0.0116	0.0063	0.0014	0.0190	0.0167	0.0037	0.0038	0.0070

Fig. 5. Charge redistribution factor ρ_{redist} in $e^{-}Ang^{-3}$ for the adhesion systems at coverage Θ = 0.25,0.5,1.0. The clean interfaces values calculated are reported in the Column "Clean".

4. Conclusions

In summary, we used an high-throughput approach to the study of the effects of the surface chemical modification on the adhesion of homogeneous metallic interfaces. This systematic approach allowed us to uncover several interesting trends. In particular, we observed that the addition of different non-metallic species at metallic interface always reduces adhesion exception made for Carbon and Boron that are adhesion enhancer. These results are supported by several experimental results in literature. Boron and Carbon in fact are well known to be used in metal casting and alloying to improve material strength, toughness, and high wear resistance and Boron more specifically is used as a grain-boundary strengthener. On the other side of the spectrum our calculations showed that P, S and in particular F are the strongest adhesion reducer. This trend too was also supported by several published works, however especially for P and S the experimental studies were more focused on lubricant additives hence their effects on the sliding behavior at the interface should be further explored. Our results show that the adhesion reducer P, S and F limit the bonding and between the slabs comprising the interface in opposite fashion with respect to C and B. This insight can be used to screen for possible molecules able to release the selected atomic species driving the tribological process and act as adhesion reduced (or enhancer). For all these adatoms an increment in their coverage leads to a competition between bonding with the substrate or between themselves. This dynamic is what underpin the non-trivial charge redistribution at the interface. Hydrogen falls outside of this general pictures and presents a unique behavior with respect to the other species, probably due to its small atomic radius. At low coverage H slightly increase adhesion on substrates that expose (110) surfaces. In all the other cases where H is presents at the interface we find a clear reduction in adhesion. In these cases the adhesion diminishes linearly with the increment of H concentration. In addition to the adhesion properties, that were the main objective of this study, we calculated the adsorption energy and work function databases for all the surfaces built during our study. These data showed that the adsorption energy is generally coverage dependent with an inverse proportionality with respect to the coverage of the adatoms (i.e. the higher the coverage the smaller is the adsorption energy). Regarding the work functions calculated for all the analyzed surfaces, we have observed that the presence of adatoms generally causes a decrease in their values. These and other important trends are outlined in the main text (and Supporting Information) and could be used as basis for further theoretical investigation or experimental work targeting the study of fictionalized surfaces. This work represents a first step in the methodical study of more realistic models of solid interfaces and their mechanical properties. Obviously the systems simulated here are still far from realistic conditions. Temperature, pressure, heterogeneity, disorder and several other factors are missing. Nonetheless the calculated quantities represent intrinsic properties that are useful to know as they represent limiting values and allow for comparisons. In fact, even considering all the limitations still present in our workflow we found several experimental work upholding our findings. Hence, this work aims to be a starting point to inform the experimental community about functional interfaces in adhesion applications. Our workflow approach can be extended (with relative ease) to include some of these parameters and support further experimental applications. In fact our future goal is to further expand our approach in order to consider a wider range of concentrations materials and heterogeneous contacts so that a well defined interface with pre-determined adhesion properties can be engineered/obtained starting from ab-initio data instead that just empirical work.

CRediT authorship contribution statement

E. Poli: Writing – review & editing, Writing – original draft, Visualization, Validation, Project administration, Methodology, Investigation, Formal analysis, Data curation, Conceptualization. **M. Cutini:** Methodology, Investigation, Conceptualization. **M.A. Nosir:** Methodology, Investigation, Data curation. **O. Chehaimi:** Software, Methodology, Data curation. **M.C. Righi:** Writing – review & editing, Writing – original draft, Supervision, Resources, Project administration, Methodology, Formal analysis, Data curation, Conceptualization.

Declaration of competing interest

The authors declare that they have no known competing financial interests or personal relationships that could have appeared to influence the work reported in this paper.

Data availability

Data will be made available on request.

Acknowledgments

These results are part of the "Advancing Solid Interface and Lubricants by First Principles Material Design (SLIDE)" project that has received funding from the European Research Council (ERC) under the European Union's Horizon 2020 research and innovation program (Grant agreement No. 865633). M.C. Righi acknowledges the European Union - NextGeneration EU (National Sustainable Mobility Center CN00000023, Italian Ministry of University and Research Decree n. 1033 - 17/06/2022, Spoke 11 - Innovative Materials & Lightweighting). The opinions expressed are those of the authors only and should not be considered as representative of the European Union or the European Commission's official position. Neither the European Union nor the European Commission can be held responsible for them.

Appendix A. Supplementary data

The Supporting Information is available free of charge. This contains the tables reporting the number of k-points, energy cutoff and number of atoms for each system simulated, the database of the d-band edges calculated for the absorption systems, the database for the DDEC charges of the Adatoms calculated for the absorption systems, the database and trends of the work function calculated for the absorption systems with and without considering the difference w.r.t. the clean surfaces of the substrates. It also contains the database and trends of the distances between slabs at the different interfaces and the correlation matrices between Bond Order and Adhesion energy and Interfacial slabs distance and adhesion energy.

Supplementary material related to this article can be found online at https://doi.org/10.1016/j.apsusc.2024.160177.

References

[1] R.A. Duine, K.-J. Lee, S.S.P. Parkin, M.D. Stiles, Synthetic antiferromagnetic spintronics, Nat. Phys. 14 (2018) 217, URL: http://dx.doi.org/10.1038/s41567-018-0050-y.

[2] Z. Tu, S. Choudhury, M.J. Zachman, S. Wei, K. Zhang, L.F. Kourkoutis, L.A. Archer, Fast ion transport at solid–solid interfaces in hybrid battery anodes, Nat. Energy 3 (2018) 310, URL: http://dx.doi.org/10.1038/s41560-018-0096-1.

[3] B. Bhushan, Nanotribology and nanomechanics in nano/biotechnology, Phil. Trans. R. Soc. A 366 (2008) 1499–1537, http://dx.doi.org/10.1098/rsta.2007.2170, URL: https://royalsocietypublishing.org/doi/abs/10.1098/rsta.2007.2170. arXiv:https://royalsocietypublishing.org/doi/pdf/10.1098/rsta.2007.2170.

[4] K. Kendall, Theoretical aspects of solid–solid Adhesion, Sci. Prog. (1933-) 72 (1988) 155–171, URL: http://www.jstor.org/stable/43420715.

[5] S.Y. Krylov, J.W.M. Frenken, The physics of atomic-scale friction: Basic considerations and open questions, Phys. Status Solidi (B) 251 (2014) 711–736, http://dx.doi.org/10.1002/pssb.201350154, URL: https://onlinelibrary.wiley.com/doi/abs/10.1002/pssb.201350154. arXiv:https://onlinelibrary.wiley.com/doi/pdf/10.1002/pssb.201350154.

[6] E. Cihan, S. İpek, E. Durgun, M.Z. Baykara, Structural lubricity under ambient conditions, Nature Commun. 7 (2016) 12055, http://dx.doi.org/10.1038/ncomms12055.

[7] S. Medina, D. Dini, A numerical model for the deterministic analysis of adhesive rough contacts down to the nano-scale, Int. J. Solids Struct. 51 (2014) 2620–2632, http://dx.doi.org/10.1016/j.ijsolstr.2014.03.033, URL: https://www.sciencedirect.com/science/article/pii/S0020768314001395.

[8] G.J.A. Müser, Meeting the contact-mechanics challenge, Tribol. Lett. 65 (2017) 118, http://dx.doi.org/10.1007/s11249-017-0900-2.

[9] D.J. Siegel, L.G. Hector, J.B. Adams, Adhesion, atomic structure, and bonding at the $Al(111)/\alpha-al_2o_3(0001)$ interface: A first principles study, Phys. Rev. B 65 (2002) 085415, http://dx.doi.org/10.1103/PhysRevB.65.085415, URL: https://link.aps.org/doi/10.1103/PhysRevB.65.085415.

[10] G. Feldbauer, M. Wolloch, P.O. Bedolla, J. Redinger, A. Vernes, P. Mohn, Suppression of material transfer at contacting surfaces: The effect of adsorbates on Al/TiN and Cu/diamond interfaces from first-principles calculations, J. Phys.: Condens. Matter 30 (2018) 105001, http://dx.doi.org/10.1088/1361-648x/aaac91.

[11] M. Tripathi, F. Awaja, R.A. Bizao, S. Signetti, E. Iacob, G. Paolicelli, S. Valeri, A. Dalton, N.M. Pugno, Friction and Adhesion of different structural defects of graphene, ACS Appl. Mater. Interfaces 10 (2018) 44614–44623, http://dx.doi.org/10.1021/acsami.8b10294.

[12] D. Cornil, N. Rivolta, V. Mercier, H. Wiame, D. Beljonne, J. Cornil, Enhanced Adhesion energy at oxide/ag interfaces for low-emissivity glasses: Theoretical insight into doping and vacancy effects, ACS Appl. Mater. Interfaces 12 (2020) 40838–40849, http://dx.doi.org/10.1021/acsami.0c07579.

[13] Q. Wang, Y. Li, Z. Chen, M. Wang, H. Zhu, H. Wang, Understanding alloying behaviors of Sc, Ni and Zn additions on Al/TiB2 interfaces based on interfacial characteristics and solute properties, Surf. Interfaces 26 (2021) 101427, http://dx.doi.org/10.1016/j.surfin.2021.101427, URL: https://www.sciencedirect.com/science/article/pii/S2468023021005046.

[14] D. Cornil, N. Rivolta, V. Mercier, H. Wiame, D. Beljonne, J. Cornil, Enhanced Adhesion energy at oxide/ag interfaces for low-emissivity glasses: Theoretical insight into doping and vacancy effects, ACS Appl. Mater. Interfaces 12 (2020) 40838–40849, http://dx.doi.org/10.1021/acsami.0c07579, arXiv:https://doi.org/10.1021/acsami.0c07579, pMID: 32804476.

[15] D. Cornil, H. Wiame, B. Lecomte, J. Cornil, D. Beljonne, Which oxide for low-emissivity glasses? First-principles modeling of silver Adhesion, ACS Appl. Mater. Interfaces 9 (2017) 18346–18354, http://dx.doi.org/10.1021/acsami.7b03269, arXiv:https://doi.org/10.1021/acsami.7b03269, pMID: 28485574.

[16] E. Rabinowicz, The determination of the compatibility of metals through static friction tests, ASLE Trans. 14 (1971) 198–205, http://dx.doi.org/10.1080/05698197108983243, arXiv:https://doi.org/10.1080/05698197108983243.

[17] J. Matějíček, M. Vilémová, R. Mušálek, P. Sachr, J. Horník, The influence of interface characteristics on the Adhesion/cohesion of plasma sprayed tungsten coatings, Coatings 3 (2013) 108–125, http://dx.doi.org/10.3390/coatings3020108, URL: https://www.mdpi.com/2079-6412/3/2/108.

[18] S. Heuer, J. Matějíček, M. Vilémová, M. Koller, K. Illkova, J. Veverka, T. Weber, G. Pintsuk, J. Coenen, C. Linsmeier, Atmospheric plasma spraying of functionally graded steel/tungsten layers for the first wall of future fusion reactors, Surf. Coat. Technol. 366 (2019) 170–178, http://dx.doi.org/10.1016/j.surfcoat.2019.03.017, URL: https://www.sciencedirect.com/science/article/pii/S0257897219302701.

[19] S. Heuer, T. Lienig, A. Mohr, T. Weber, G. Pintsuk, J. Coenen, F. Gormann, W. Theisen, C. Linsmeier, Ultra-fast sintered functionally graded fe/w composites for the first wall of future fusion reactors, Composites B 164 (2019) 205–214, http://dx.doi.org/10.1016/j.compositesb.2018.11.078, URL: https://www.sciencedirect.com/science/article/pii/S1359836818313611.

[20] F. Ding, P. Larsson, J.A. Larsson, R. Ahuja, H. Duan, A. Rosén, K. Bolton, The importance of strong carbon metal Adhesion for catalytic nucleation of single-walled carbon nanotubes, Nano Lett. 8 (2008) 463–468, http://dx.doi.org/10.1021/nl072431m, arXiv:https://doi.org/10.1021/nl072431m.

[21] Z. Hafsi, M. Mishra, S. Elaoud, Hydrogen embrittlement of steel pipelines during transients, Procedia Struct. Integr. 13 (2018) 210–217, http://dx.doi.org/10.1016/j.prostr.2018.12.035, URL: https://www.sciencedirect.com/science/article/pii/S2452321618302683.

[22] M. Louthan, G. Caskey, Hydrogen transport and embrittlement in structural metals, Int. J. Hydrogen Energy 1 (1976) 291–305, http://dx.doi.org/10.1016/0360-3199(76)90024-0, URL: https://www.sciencedirect.com/science/article/pii/0360319976900240.

[23] A. Ayyagari, K.I. Alam, D. Berman, A. Erdemir, Progress in superlubricity across different media and material systems—a review, Front. Mech. Eng. 8 (2022) http://dx.doi.org/10.3389/fmech.2022.908497, URL: https://www.frontiersin.org/articles/10.3389/fmech.2022.908497.

[24] L. Pang, A. Barras, V. Mishyn, G. Sandu, S. Melinte, P. Subramanian, R. Boukherroub, S. Szunerits, Enhanced electrocatalytic hydrogen evolution on a plasmonic electrode: the importance of the ti/tio2 Adhesion layer, J. Mater. Chem. A 8 (2020) 13980–13986, http://dx.doi.org/10.1039/D0TA02353A.

[25] S. Curtarolo, G.L.W. Hart, M.B. Nardelli, N. Mingo, S. Sanvito, O. Levy, The high-throughput highway to computational materials design, Nature Mater. 12 (2013) 191–201, http://dx.doi.org/10.1038/nmat3568, URL: https://www.nature.com/articles/nmat3568.

[26] S. Haastrup, M. Strange, M. Pandey, T. Deilmann, P.S. Schmidt, N.F. Hinsche, M.N. Gjerding, D. Torelli, P.M. Larsen, A.C. Riis-Jensen, J. Gath, K.W. Jacobsen, J.J. Mortensen, T. Olsen, K.S. Thygesen, The computational 2d materials database: high-throughput modeling and discovery of atomically thin crystals, 2D Mater. 5 (2018) 042002, http://dx.doi.org/10.1088/2053-1583/aacfc1, URL: https://iopscience.iop.org/article/10.1088/2053-1583/aacfc1.

[27] Z. Li, J. Yoon, R. Zhang, F. Rajabipour, W.V. Srubar III, I. Dabo, A. Radlińska, Machine learning in concrete science: applications, challenges, and best practices, NPJ Comput. Mater. 8 (2022) 127, http://dx.doi.org/10.1038/s41524-022-00810-x.

[28] A.S. Rosen, V. Fung, P. Huck, C.T. O'Donnell, M.K. Horton, D.G. Truhlar, K.A. Persson, J.M. Notestein, R.Q. Snurr, High-throughput predictions of metal–organic framework electronic properties: theoretical challenges, graph neural networks, and data exploration, NPJ Comput. Mater. 8 (2022) 112, http://dx.doi.org/10.1038/s41524-022-00796-6.

[29] O.L. Hebnes, M.E. Bathen, Ø.S. Schøyen, S.G. Winther-Larsen, L. Vines, M. Hjorth-Jensen, Predicting solid state material platforms for quantum technologies, NPJ Comput. Mater. 8 (2022) 207, http://dx.doi.org/10.1038/s41524-022-00888-3.

[30] G. Losi, O. Chehaimi, M.C. Righi, Tribchem: A software for the first-principles, high-throughput study of solid interfaces and their tribological properties, J. Chem. Theory Comput. 19 (2023) 5231–5241, http://dx.doi.org/10.1021/acs.jctc.3c00459, arXiv:https://doi.org/10.1021/acs.jctc.3c00459.

[31] M. Wolloch, G. Levita, P. Restuccia, M.C. Righi, Interfacial charge density and its connection to Adhesion and frictional forces, Phys. Rev. Lett. 121 (2018) 026804, http://dx.doi.org/10.1103/PhysRevLett.121.026804, URL: https://link.aps.org/doi/10.1103/PhysRevLett.121.026804.

[32] A. Jain, S.P. Ong, W. Chen, B. Medasani, X. Qu, M. Kocher, M. Brafman, G. Petretto, G.-M. Rignanese, G. Hautier, D. Gunter, K.A. Persson, Fireworks: a dynamic workflow system designed for high-throughput applications, Concurr. Comput.: Pract. Exper. 27 (2015) 5037–5059, http://dx.doi.org/10.1002/cpe.3505.

[33] K. Mathew, J.H. Montoya, A. Faghaninia, S. Dwarakanath, M. Aykol, H. Tang, I. heng Chu, T. Smidt, B. Bocklund, M. Horton, J. Dagdelen, B. Wood, Z.-K. Liu, J. Neaton, S.P. Ong, K. Persson, A. Jain, Atomate: A high-level interface to generate, execute, and analyze computational materials science workflows, Comput. Mater. Sci. 139 (2017) 140–152, http://dx.doi.org/10.1016/j.commatsci.2017.07.030, URL: https://www.sciencedirect.com/science/Article/pii/S0927025617303919.

[34] S.P. Ong, W.D. Richards, A. Jain, G. Hautier, M. Kocher, S. Cholia, D. Gunter, V.L. Chevrier, K.A. Persson, G. Ceder, Python materials genomics (pymatgen): A robust, open-source python library for materials analysis, Comput. Mater. Sci. 68 (2013) 314–319, http://dx.doi.org/10.1016/j.commatsci.2012.10.028, URL: https://www.sciencedirect.com/science/Article/pii/S0927025612006295.

[35] K. Mathew, A.K. Singh, J.J. Gabriel, K. Choudhary, S.B. Sinnott, A.V. Davydov, F. Tavazza, R.G. Hennig, Mpinterfaces: A materials project based python tool for high-throughput computational screening of interfacial systems, Comput. Mater. Sci. 122 (2016) 183–190, http://dx.doi.org/10.1016/j.commatsci.2016.05.020, URL: http://www.sciencedirect.com/science/Article/pii/S0927025616302440.

[36] G. Kresse, J. Furthmuller, Efficient iterative schemes for ab initio total-energy calculations using a plane-wave basis set, Phys. Rev. B 54 (1996) 11169–11186, http://dx.doi.org/10.1103/PhysRevB.54.11169, URL: https://link.aps.org/doi/10.1103/PhysRevB.54.11169.

[37] G. Kresse, D. Joubert, From ultrasoft pseudopotentials to the projector augmented-wave method, Phys. Rev. B 59 (1999) 1758–1775, http://dx.doi.org/10.1103/PhysRevB.59.1758, URL: https://link.aps.org/doi/10.1103/PhysRevB.59.1758.

[38] J.P. Perdew, K. Burke, M. Ernzerhof, Generalized gradient approximation made simple, Phys. Rev. Lett. 77 (1996) 3865–3868, http://dx.doi.org/10.1103/PhysRevLett.77.3865, URL: https://link.aps.org/doi/10.1103/PhysRevLett.77.3865.

[39] N.G. Limas, T.A. Manz, Introducing ddec6 atomic population analysis: part 4. efficient parallel computation of net atomic charges, atomic spin moments, bond orders, and more, RSC Adv. 8 (2018) 2678–2707, http://dx.doi.org/10.1039/C7RA11829E.

[40] T.A. Manz, Introducing ddec6 atomic population analysis: part 3. Comprehensive method to compute bond orders, RSC Adv. 7 (2017) 45552–45581, http://dx.doi.org/10.1039/C7RA07400J.

[41] V. Wang, N. Xu, J.-C. Liu, G. Tang, W.-T. Geng, Vaspkit: A user-friendly interface facilitating high-throughput computing and analysis using vasp code, Comput. Phys. Comm. 267 (2021) 108033, http://dx.doi.org/10.1016/j.cpc.2021.108033, URL: https://www.sciencedirect.com/science/article/pii/S0010465521001454.

[42] M. Chandross, N. Argibay, Friction of metals: A review of microstructural evolution and nanoscale phenomena in shearing contacts, Tribol. Lett. 69 (2017) 119, http://dx.doi.org/10.1007/s11249-021-01477-z.

[43] T.E. Fischer, Tribochemistry, Annu. Rev. Mater. Res. 18 (1988) 303–323, http://dx.doi.org/10.1146/annurev.ms.18.080188.001511, URL: https://www.annualreviews.org/content/journals/10.1146/annurev.ms.18.080188.001511.

[44] S. Mori, Y. Shitara, Tribochemical activation of gold surface by scratching, Appl. Surf. Sci. 78 (1994) 269–273, http://dx.doi.org/10.1016/0169-4332(94)90014-0, URL: https://www.sciencedirect.com/science/article/pii/0169433294900140.

[45] M.I. De Barros-Bouchet, M.C. Righi, D. Philippon, S. Mambingo-Doumbe, T. Le-Mogne, J.M. Martin, A. Bouffet, Tribochemistry of phosphorus additives: experiments and first-principles calculations, RSC Adv. 5 (2015) 49270–49279, http://dx.doi.org/10.1039/C5RA00721F.

[46] D. Philippon, M.-I. De Barros-Bouchet, T. Le Mogne, O. Lerasle, A. Bouffet, J.-M. Martin, Role of nascent metallic surfaces on the tribochemistry of phosphite lubricant additives, Tribol. Int. 44 (2011) 684–691, http://dx.doi.org/10.1016/j.triboint.2009.12.014, URL: https://www.sciencedirect.com/science/article/pii/S0301679X0900351X. special Issue on Boundary Lubrication.

[47] S. Peeters, C. Charrin, I. Duron, S. Loehlé, B. Thiebaut, M. Righi, Importance of the catalytic effect of the substrate in the functionality of lubricant additives: the case of molybdenum dithiocarbamates, Mater. Today Chem. 21 (2021) 100487, http://dx.doi.org/10.1016/j.mtchem.2021.100487, URL: https://www.sciencedirect.com/science/article/pii/S2468519421000677.

[48] J.K. Nørskov, F. Abild-Pedersen, F. Studt, T. Bligaard, Density functional theory in surface chemistry and catalysis, Proc. Natl. Acad. Sci. 108 (2011) 937–943, http://dx.doi.org/10.1073/pnas.1006652108, URL: https://www.pnas.org/doi/abs/10.1073/pnas.1006652108. arXiv:https://www.pnas.org/doi/pdf/10.1073/pnas.1006652108.

[49] B. Hammer, J. Nørskov, Electronic factors determining the reactivity of metal surfaces, Surf. Sci. 343 (1995) 211–220, http://dx.doi.org/10.1016/0039-6028(96)80007-0, URL: https://www.sciencedirect.com/science/article/pii/0039602896800070.

[50] B. Hammer, J.K. Nørskov, Why gold is the noblest of all the metals, Nature 376 (1995) 238–240, http://dx.doi.org/10.1038/376238a0.

[51] P. Restuccia, G. Losi, O. Chehaimi, M. Marsili, M.C. Righi, High-throughput first-principles prediction of interfacial Adhesion energies in metal-on-metal contacts, ACS Appl. Mater. Interfaces 15 (2023) 19624–19633, http://dx.doi.org/10.1021/acsami.3c00662, arXiv:https://doi.org/10.1021/acsami.3c00662, pMID: 37015021.

[52] A. Bhunia, Boron has more surprises, Chem 6 (2020) 320–321, http://dx.doi.org/10.1016/j.chempr.2020.01.017, URL: https://www.sciencedirect.com/science/article/pii/S2451929420300413.

[53] L. Qiu, X. Zhang, X. Kong, I. Mitchell, T. Yan, S.Y. Kim, B.I. Yakobson, F. Ding, Theory of sigma bond resonance in flat boron materials, Nature Commun. 14 (2023) 1804, http://dx.doi.org/10.1038/s41467-023-37442-8.

[54] N. Nyholm, N. Espallargas, Functionalized carbon nanostructures as lubricant additives – a review, Carbon 201 (2023) 1200–1228, http://dx.doi.org/10.1016/j.carbon.2022.10.035, URL: https://www.sciencedirect.com/science/article/pii/S0008622322008569.

[55] K. Zhang, Y. Zhang, L. Shi, A review of linear carbon chains, Chin. Chem. Lett. 31 (2020) 1746–1756, http://dx.doi.org/10.1016/j.cclet.2020.03.019, URL: https://www.sciencedirect.com/science/article/pii/S1001841720301388.

[56] Z. Li, C. Xu, G. Xiao, J. Zhang, Z. Chen, M. Yi, Lubrication performance of graphene as lubricant additive in 4 n pentyl 4 cyanobiphyl liquid crystal (5cb) for steel/steel contacts, Materials 11 (2018) URL: https://www.mdpi.com/1996-1944/11/11/2110.

[57] D. Berman, A. Erdemir, A.V. Sumant, Graphene: a new emerging lubricant, Mater. Today 17 (2014) 31–42, http://dx.doi.org/10.1016/j.mattod.2013.12.003, URL: https://www.sciencedirect.com/science/article/pii/S1369702113004574.

[58] M. Izaki, N. Miyamoto, A. Nakae, T. Hasegawa, S. Watase, M. Chigane, Y. Fujiwara, M.I.H. Enomoto, Martensitic iron-carbon-boron alloy electrodeposit with improved mechanical properties, J. Electrochem. Soc. 149 (2002) C370, http://dx.doi.org/10.1149/1.1484376.

[59] Z. Li Liu, X. Chen, Y. Xiang, K. Li, H.U. Hua, High boron iron-based alloy and its modification, J. Iron Steel Res. Int. 16 (2009) 37–54, http://dx.doi.org/10.1016/S1006-706X(09)60041-8, URL: https://www.sciencedirect.com/science/article/pii/S1006706X09600418.

[60] A. Sharma, S. Dixit, N. Baler, P. Agrawal, S.K. Makineni, K. Chattopadhyay, Impact of boron as an alloying addition on the microstructure, thermo-physical properties and creep resistance of a tungsten-free co-base superalloy, Mater. Sci. Eng. A 855 (2022) 143899, http://dx.doi.org/10.1016/j.msea.2022.143899, URL: https://www.sciencedirect.com/science/article/pii/S0921509322012783.

[61] S. Ma, J. Zhang, Wear resistant high boron cast alloy - a review, Rev. Adv. Mater. Sci. 44 (2016) 54–62, URL: https://www.ipme.ru/e-journals/RAMS/no_14416/05_14416_zhang.pdf.

[62] C. Garcia-Cabezon, C. Garcia-Hernandez, M.L. Rodriguez-Mendez, G. Herranz, F. Martin-Pedrosa, Role of carbon and nitrogen in the improvement of corrosion resistanceof new powder metallurgy co-cr-mo alloys, Corros. Rev. 38 (2020) 273–286, http://dx.doi.org/10.1515/corrrev-2019-0109.

[63] A. Szkliniarz, W. Szkliniarz, Carbon in commercially pure titanium, Materials 16 (2023) URL: https://www.mdpi.com/1996-1944/16/2/711.

[64] Y. Chen, P. Renner, H. Liang, A review of current understanding in tribo-chemical reactions involving lubricant additives, Friction 11 (2023) 489–512, http://dx.doi.org/10.1007/s40544-022-0637-2, URL: https://www.sciopen.com/article/10.1007/s40544-022-0637-2.

[65] A.A. Mohamed Faruck, C.-J. Hsu, N. Doerr, M. Weigand, C. Gachot, How lubricant formulations and properties influence the performance of rotorcraft transmissions under loss of lubrication conditions, Tribol. Int. 151 (2020) 106390, http://dx.doi.org/10.1016/j.triboint.2020.106390, URL: https://www.sciencedirect.com/science/article/pii/S0301679X20302279.

[66] A.E. Somers, S.M. Biddulph, P.C. Howlett, J. Sun, D.R. MacFarlane, M. Forsyth, A comparison of phosphorus and fluorine containing il lubricants for steel on aluminium, Phys. Chem. Chem. Phys. 14 (2012) 8224–8231, http://dx.doi.org/10.1039/C2CP40736A.

[67] S. Veldhuis, G. Dosbaeva, G. Benga, Application of ultra-thin fluorine-content lubricating films to reduce tool/workpiece adhesive interaction during thread-cutting operations, Int. J. Mach. Tools Manuf. 47 (2007) 521–528, http://dx.doi.org/10.1016/j.ijmachtools.2006.06.003, URL: https://www.sciencedirect.com/science/article/pii/S0890695506001441.

[68] C.S. Ware, T. Smith-Palmer, S. Peppou-Chapman, L.R.J. Scarratt, E.M. Humphries, D. Balzer, C. Neto, Marine antifouling behavior of lubricant-infused nanowrinkled polymeric surfaces, ACS Appl. Mater. Interfaces 10 (2018) 4173–4182, http://dx.doi.org/10.1021/acsami.7b14736, arXiv:https://doi.org/10.1021/acsami.7b14736, pMID: 29250952.

[69] G. Fatti, M.C. Righi, Selenium chemisorption makes iron surfaces slippery, Tribol. Lett. 7 (2019) 125, http://dx.doi.org/10.1007/s11249-019-1235-y.

[70] S.K. Dwivedi, M. Vishwakarma, Hydrogen embrittlement in different materials: A review, Int. J. Hydrogen Energy 43 (2018) 21603–21616, http://dx.doi.org/10.1016/j.ijhydene.2018.09.201, URL: https://www.sciencedirect.com/science/article/pii/S0360319918331306.